WWOX Regulates UV/Cold Shock-Mediated Calcium Influx and Nuclear Bubbling in Frostbite

Cheng-Chang Tsai
National Cheng Kung University

Szu-Jung Chen
National Cheng Kung University

Wen-Ting Deng
National Cheng Kung University

Tsung-Yun Liu
National Cheng Kung University

Kuan-Ting Lee
National Cheng Kung University

Ming-Hui Lee
National Cheng Kung University

Sing-Ru Lin
National Cheng Kung University

Yu-An Chen
National Cheng Kung University

Lu-Hai Wang
China Medical University

Li-Jen Su
National Central University

Hamm-Ming Sheu
National Cheng Kung University

Nan-Shan Chang (✉ nschang13827@gmail.com)
National Cheng Kung University   https://orcid.org/0000-0002-6889-8756

Article

Abstract

UV/cold shock-mediated frostbite involves non-apoptotic nuclear bubbling cell death (BCD) and participation of functional WWOX in cells (WWOXf). In contrast, cells with WWOX deficiency or dysfunction (WWOXd) undergo pop-out explosion death (POD). Here, by time-lapse microscopy, when WWOXf cells were exposed to UV or UV/cold shock and then incubated at room temperature, these cells rapidly and sequentially underwent: 1) loss of mitochondrial membrane potential, 2) formation of a nitric oxide (NO)-containing nuclear bubble per cell, 3) WWOX-dependent increase in calcium (Ca^{2+}) influx, 4) shutdown of mRNA and protein synthesis machinery, as determined by RT/PCR and gene chip analysis, and 5) eventual cell death without caspase activation, stress fiber formation and chromosomal DNA fragmentation. In contrast, WWOXd cells exhibited a faster kinetics of stress fiber formation, explosion and death without NO production. Ectopic WWOX restored calcium influx and nuclear bubbling in WWOXd cells. In hairless mice, UV/cold shock rapidly downregulated protein expression in the skin and then liver, which may lead to organ damages. UV/cold shock induced complex formation of antiapoptotic TRAF2 and proapoptotic WWOX and their co-translocation to the nucleus, where the complex dissociation occurred. The observations suggest that WWOX and TRAF2 dissociation is needed for nuclear bubbling and death.

Introduction

In contrast to the caspase-dependent programmed cell death such as apoptosis[1−8] or caspase-independent necrosis[9,10], we have previously reported nucleus-initiated cell death, designated bubbling cell death (BCD)[11,12]. To begin with, increased human travel to the outer space is expected in the near future. If accident occurs during the travel, humans are likely to get exposed to strong ultraviolet irradiation such as UVC (wavelength 100 to 280 nm) and extreme cold shock. We determined that when temperature is lowered in the surrounding environment, dying cells do not undergo apoptosis and yet they undergo BCD[11,12]. Here, our study concerns the severity of frostbite and UV irradiation in the polar regions and even outer space[11,12]. When exposed to severe cold and strong UV irradiation, people suffer serious damages to their skin and leading to damage in internal organs, and eventually results in limb amputations, organ failure, and even death. BCD has been defined as "formation of a single bubble from the nucleus per cell and release of this swelling bubble from the cell surface to extracellular space that irreversibly causes cell death" [11,12]. When cells are subjected to UV irradiation and/or brief cold shock (4°C for 5 min) and then incubated at room temperature or 4°C for time-lapse microscopy, each cell releases an enlarging nuclear gas bubble containing nitric oxide (NO). Certain cells may simultaneously eject hundreds or thousands of extracellular vesicles (EV) or exosome-like particles. Unlike apoptosis, BCD does not exhibit membrane phosphatidylserine flip-over, mitochondrial apoptosis, damage to Golgi complex, and chromosomal DNA fragmentation. When the temperature is increased back at 37°C, BCD stops and apoptosis starts[11,12]. Indeed, BCD can occur at 37°C. For example, when cells are transiently overexpressed with the Hyal-2/WWOX/Smad4 signaling complex, hyaluronan induces BCD at 37°C[13].

Most recently, we reported that metastatic cancer cells are frequently deficient in WWOX protein or express dysfunctional WWOX (designated WWOXd)[14]. WWOXd cells are less efficient in generating calcium (Ca^{2+}) influx and undergo non-apoptotic explosion or pop-out death (POD) in response to UV irradiation in room temperature. However, UV induced functional WWOX-expressing cells (designated WWOXf) to undergo BCD, along with an efficient Ca^{2+} influx. WWOXf cells migrate collectively and expel the individually migrating WWOXd cells. WWOXd cells in turn induce apoptosis of WWOXf cells without physical contact[14,15]. In this study, we continued to examine the underlying mechanisms and showed that UV caused WWOXf cells to rapidly decrease mitochondrial membrane potential and increase NO and reactive oxygen species (ROS), followed by formation of NO-containing nuclear bubbles, calcium influx, and death without caspase activation. Structural analysis revealed that the first WW domain of WWOX was essential for calcium influx and nuclear bubble formation. Shutdown of the cellular mRNA synthesis, translation machinery and protein synthesis, but not stress fiber formation, occurred in WWOXf cells and hairless mice. Compared to WWOXf cells, WWOXd cells could not effectively generate NO gas but had increased stress fiber formation prior to death. WWOXd died faster than that of WWOXf cells. Participation of proapoptotic WWOX and p53 axis is counteracted by antiapoptotic TRAF2 was examined in WWOXf cells.

Results

WWOXf cells undergo nuclear bubbling or BCD at room temperature and below. WWOXf cells undergo nuclear bubbling and death in response to UV or UV/cold shock[11,12]. A panel of WWOXf cells used for experiments were TNF-sensitive L929S fibroblasts, human breast MCF7 cells, monkey kidney COS7 fibroblasts, prostate DU145 cancer cells, and squamous cell carcinoma SCC9 and SCC15 cells[14]. When TNF-sensitive L929S fibroblasts were exposed to UV irradiation (480 mJoule/cm^2) and then cold shock at 4°C for indicated times, the cells underwent time-related bubbling (see arrows for bubbles; Fig. 1a).

The aforementioned cells were exposed to UV only, UV then cold shock (4°C for 5 min), or cold shock then UV. Post treatment, these cells were cultured at 4, 10, 22, and 37°C, respectively, for indicated times (Fig. 1b-g). Nuclear bubbling of MCF7 cells occurred most effectively at 22°C or room temperature (Fig. 1b-d; Supplementary Video 1), and bubbling blocked at 37°C by greater than 70%. For L929S cells, 4°C was the best temperature for UV-mediated nuclear bubbling (Fig. 1e-g). In stark contrast, WWOXd MDA-MB-231, MDA-MB-231(NH) and metastatic MDA-MB-231 cells (IV-2-3) were UV irradiated and then cold shocked, and underwent POD at all indicated temperatures (Fig. 1h-j; Supplementary Video 2). Triple-negative breast MDA-MB-231 do not express estrogen receptor (ER), progesterone receptor (PR), and human epidermal growth factor receptor 2 (HER2), whereas MCF7 is ER positive[16].

Similarly, COS7 cells underwent UV/cold shock-mediated nuclear bubbling, and the bubbling reduced at 37°C (Supplementary Fig. 1a). In response to UV only or UV and then cold shock, WWOXd TNF-resistant L929R fibroblasts underwent pop-out explosion at 10 and 22°C, and the explosion retarded at 37°C (Supplementary Fig. 1b). Again, POD ocurred in MDA-MB-231(NH) and MDA-MB-231 (IV-2-3) cells upon

exposure to UV only (Supplementary Fig. 1c). Similar results were observed when MDA-MB-231 cells treated with cold shock and then UV (Supplementary Fig. 1c). Temperature changes failed to alter the extent of POD (Supplementary Fig. 1c).

Failure in trypan blue exclusion and mitochondrial respiration during BCD. When cells start undergoing nuclear bubbling, nuclear permeability is increased as indicated by the presence of DAPI, but not propidium iodide (PI), in the nuclei[11]. When the bubble enlarges to a certain extent, PI uptake in the nuclei occurs, indicating that the cell is dead[11]. When COS7 cells were exposed to UV and incubated at room temperature for 2 hour, the cells failed to exclude trypan blue (see red arrows; Supplementary Fig. 2a). Similar results were observed in UV/cold shock-treated COS7 cells (Supplementary Fig. 2b).

Rapid loss of miotchondrial function occurred in UV-treated COS7 cells, as determined by MTT assay (Supplementary Fig. 2c). Dramatically functional loss occurred if UV-irradiated cells were cultured overnight at 37°C (Supplementary Fig. 2d). Unlike apoptosis, BCD is an irreverible cell death event[11,12]. COS7 cells were UV irradiated and then cultured at 4, 22, or 37°C for various durations. Subculture of these cells for overnight incubation at 37°C resulted in cell death by >90% (Supplementary Fig. 2e). Similar results were observed when these UV-treated cells were direclty cultured overnight at 37°C (Supplementary Fig. 2f). Rapid suppression of mitochondrial function was observed when the UV-treated COS7 cells were cultured at 4°C for 1-4 hr, compared to other temperatures (Supplementary Fig. 2g).

Next, COS7 cells were treated with betulinic acid (10 µM) or staurosporine (1 µM) for 1 hour to initiate mitochondrial apoptosis, then exposed to UV and cold shock (4°C for 5 min), and incubated at room temperature for indicated times. Compared to UV/cold shock-treated cells, pre-induction of mitochondrial apoptosis did not block BCD (Supplementary Fig. 2h). Pre-inhibition of caspases by caspase inhibitor I (z-VAD-FMK) or caspase inhibitor X (specific for caspase 3, 7, and 8) failed to block BCD (Supplementary Fig. 2h). Internucleosomal DNA fragmentation was not detected in UV/cold shock-treated cells during incubation at RT (Supplementary Fig. 2i). When L929S, but not COS7, were exposed to UV and then culturing at 37°C for 8 hr, DNA fragmentation occurred (Supplementary Fig. 2j, k). As positive controls, staurosporine at 1 µM induced DNA fragmentation at 37°C but not at RT or 4°C (Supplementary Fig. 2j, k). Failure of UV-treated COS7 to undergo DNA fragmentation during incubation for 8 hr at 37°C was probably due to insufficient incubation time.

Inhibitors of necroptosis fail to block UV/cold shock-induced BCD in WWOXf cells and POD in WWOXd cells

When L929S cells were pretreated with a necroptosis inhibitor Nec-1 (30 µM) for 1 hr and then exposed to UV (480 mJoule/cm^2) and cold shock for 5 min at 4° C, the treated cells exhibited bubbling in 1.5 hr (Supplementary Fig. 3; Supplementary Table I). Similar results were observed by using a protein synthesis inhibitor actinomycin D (ActD; Supplementary Table I).

Supplementary Table I shows the detailed characteristics of BCD and POD, including cell shrinkage, release of nucleolar contents, nuclear bubbling, and release of extracellular vesicles. Release of nucleolar content occurred just prior to bubbling from the nucleus (Supplementary Table I; Supplementary Video 1). ActD delayed the release of nucleolar content. Pretreatment of L929S cells with necroptosis inhibitors Nec-1 and GSK'872 for 30 min failed to abolish the nuclear bubbling (Supplementary Fig. 3a). Under similar conditions, L929R cells underwent POD without nuclear bubbling (Supplementary Fig. 3b). Also, Nec-1 had no effects (Supplementary Fig. 3b; Supplementary Table I). Oral squamous cell carcinoma SCC15 and SCC9 are WWOXf cell lines[7,14]. These cells underwent BCD in response to UV or UV/cold shock (Supplementary Table I). ActD and β-mercaptoethanol (10%) abolished UV/cold shock-mediated release of nucleolar content.

Antioxidant U74389G suppresses BCD in WWOXf cells at RT

UV/cold shock induces translocation of nitric oxide synthase 2 (NOS2) to the nucleus to generate nitric oxide (NO) for causing nuclear bubbling[11,12]. To further elucidate the nuclear bubbling, SCC15 cells were pretreated with EGTA (1 mM), proteasome inhibitor MG132 (30 μM), p53 activator Prima-1 (30 μM), CHK2/ATM inhibitor (30 μM), or antioxidant U74389G (30 μM) for 30 min. These cells were exposed to UV irradiation (480 mJoule/cm^2) or UV/cold shock (5 min at 4°C). By time-lapse microscopy at room temperature, U74389G strongly suppressed the nuclear bubbling (Supplementary Fig. 4). EGTA, a calcium ion chelator, also retarded the occurrence of BCD (Supplementary Fig. 4). Antioxidant U74389G is an inhibitor of free radical production and lipid peroxidation and caspase 1[17,18].

Dramatic increases in cellular thickness or height during apoptosis, but not BCD, as determined by time-lapse holographic microscopy

Holographic microscopy allows visualization of three-dimensional changes of cells undergoing division, apoptosis and others[19]. When COS7 or L929S cells were exposed to UV and then cold shock at various durations at 4°C, cell bubbling were observed (Fig. 2a; Supplementary Videos 3, 4). The thickness or heights of cell bubbles were relatively low in COS7 and L929S cells during BCD (less than 2 μm; Fig. 2b, c; Supplementary Video 5). When L929S cells were treated with staurosporine and cultured at 37 °C, cells underwent apoptosis, which showed shrinkage and increased whole cell thickness reaching ~12 μm (Fig. 2d; Supplementary Video 6). In comparison, when UV/cold shock-treated L929S cells were cultured at 37°C, apoptosis occurred and the cell bubble heights reached ~15 μm (Supplementary Video 7). During cell division, L929S cells reached as tall as ~17 μm (Supplementary Videos 8, 9). Thus, during BCD, there were brief increases in cell volumes followed by reduction, and cell areas remained relatively stable (Fig. 2e). When cells underwent apoptosis, cell areas and volumes were reduced. However, cells became taller, which lasted for 5-8 hr (Fig. 2e).

UV induces WWOXf cells to rapidly lose mitochondrial membrane potential and meanwhile increase the production of nitric oxide (NO)

UV treatment leads WWOXf cells to undergo nuclear bubbling and calcium (Ca^{2+}) influx and eventual death, whereas UV causes WWOXd cells to explode in 30 min with a poor efficiency in Ca^{2+} influx[14]. By using live cell dyes for time-lapse microscopy (Fig. 3), UV-treated L929S cells exhibited 1) rapid loss of mitochondrial membrane potential (using MitoTracker Red) (Fig. 3a, b, e, f), 2) reduction in cell survival from low retention of calcein dye (Fig. 3b), 3) rapid increase in the production of ROS (Dichlorofluorescein dye) (Fig. 3a) and NO (DAF-fm diacetate dye) (Fig. 3c), and 4) relatively low in stress fiber formation (Phalloidin green dye) (Fig. 3e). UV-mediated bubbling initiation occurred approximately in 30 min in L929S cells, whereas whole cell explosion occurred in L929R in less than 30 min. UV induced L929R cells to form stress fibers after whole cell explosion in less than 30 min, but not in L929S cells (Fig. 3e). Many other WWOXd cells were readily to form UV-induced stress fibers, whereas WWOXf cells failed to do so. No apparent changes were shown with intracellular utilization of ATP (BioTracker ATP-Red Live Cell Dye), incorporation of NTP (BioTracker Red NTP Transporter), and changes in cell stemness (BioTracker 529 Green Pluripotent Stem Cell Dye) in both L929S and L929R cells (Fig. 3d). NO levels were 2.5-fold higher in L929S than in L929R cells (Fig. 3c).

Calcein retention for measuring survival was better in WWOXf L929S (Fig. 3b) and lung WWOXf H441 cells (Fig. 3h), but not in WWOXd L929R (Fig. 3b) and lung H661 cells (Fig. 3h). UV-induced Ca^{2+} influx (Fluo-8 dye) was shown in WWOXf H441 (Fig. 3g) and NCI-H1299 cells (Fig. 3i), but not in WWOXd H661 (Fig. 3g) and PC9 cells (Fig. 3i). Next, compared to non-sphere areas in the 4T1 monolayers, 4T1 spheres had higher levels of ROS (Fig. 3j. left panel) and stemness (Fig. 3k), but not NO (Fig. 3j, right panel). A typical 4T1 sphere is shown (Fig. 3l). Finally, DAPI (nuclear dye) uptake occurred in a time-related manner with similar kinetics in all cells (Fig. 3).

p53, WWOX and p38, but not TβRI, participate in UV-mediated nuclear bubbling and calcium influx in WWOXf cells

UV or UV/cold shock initiates nuclear bubbling and calcium influx, which takes approximately 30 min in WWOXf cells (e.g. L929S) at room temperature[14]. We examined how both events occur in WWOXf HCT116 cells. In the control experiments (Fig. 4a1-3), HCT116 cells were cultured overnight and added a 100 µl aliquot of medium, PBS, or normal rabbit serum (1:250 dilution). UV caused the initiation of nuclear bubbling and calcium influx in approximately 30 min at room temperature (Fig. 4a1-3). Calcium influx reached maximally in about an hour, followed by reduction with time (Fig. 4a1-2). In contrast, normal rabbit serum sustained the increase in calcium influx with time (Fig. 4a3).

When HCT116 cells were pretreated with calcium chelator EGTA at 200 µM for 1 hr, calcium influx was not effectively blocked and the first bubbling time was prolonged to approximately 48 min (Fig. 4a4). To be effective, greater than 1 mM EGTA was needed to achieve 50% inhibition of calcium influx. As an inhibitor of NO synthase, Nω-nitro-L-arginine methyl ester hydrochloride (Nω-LAME) at 300 µM retarded

the nuclear bubbling but had no effect on calcium influx (Fig. 4a5), suggesting that NO is needed for bubbling but not for calcium influx. To suppress >50% nuclear bubbling, 1 mM Nω-LAME is needed[11].

We examined whether WWOX and its binding protein partners such as p53, type II TGFβ receptor (TβRII) and Hyal-2 participate in calcium influx and nuclear bubbling[20–25]. p53 wild type and isoforms such as p53β and p53γ have been implicated in cancer progression[26,27]. Firstly, we examined the role of p53 and isoforms (Fig. 4b1-4). When HCT116 cells were pretreated with an aliquot of antiserum against p53 (1 μg/ml) followed by exposure to UV, the antibody did not block nuclear bubbling but partially inhibited calcium influx (Fig. 4b1). In contrast, polyclonal p53 antibody (1 μg/ml) was potent in blocking both events (Fig. 4b2). In contrast, p53β or p53γ antibody retarded the nuclear bubbling but not calcium influx (Fig. 4b3-4). The observations suggest that wild type p53 participate in both nuclear bubbling and calcium influx, whereas p53β and p53γ are needed for nuclear bubbling.

Secondly, we investigated the role of TGFβ receptor (TβR) on both aforementioned events (Fig. 4c1-3). HCT116 cells are deficient in type II TGFβ receptor (TβRII)[28]. HCT116 cells were pretreated with a chemical inhibitor for TβRI for 30 min and then UV exposure. The treatment did not result in inhibition of calcium influx and nuclear bubbling (Fig. 4c1). Also, monoclonal antibody against TβRII did not alter UV-mediated responses in HCT116 cells (Fig. 4c2). The chemical inhibitor SD208 for TβRI had no apparent inhibitory effects (Fig. 4c3).

Thirdly, we examined the effect of WWOX protein on the UV-mediated cellular responses (Fig. 4d1-13). WWOX7-21 and WWOX7-11 peptides enhance ceritinib-mediated breast cancer cell death[24,25]. When HCT116 cells were pretreated with either WWOX7-21 or WWOX7-11 peptide (20 μM) for 30 min and then exposed to UV, there were no apparent changes in nuclear bubbling and calcium influx (Fig. 4d1-2). Similar results were observed using mutant peptides WWOX7-11(A7R) and WWOX7-11(G7R) (Fig. 4d3-4). Three antibodies against indicated different regions of WWOX at amino acid 7-21, 28-42 and 286-299, respectively, have been made[20–22, 29]. These antibodies retarded calcium influx but had no effect on nuclear bubbling (Fig. 4d5-7). Antibodies against WWOX phosphorylation sites, including pY33, pT12 and pS14-WWOX, strongly blocked calcium influx, whereas pY34 and pY287-WWOX antibodies were partially effective (Fig. 4d8-12). pS14-WWOX strongly retarded nuclear bubbling (Fig. 4d11). Antibody against isoform WWOX2 suppressed calcium influx but failed to block nuclear bubbling (Fig. 4d13). The observations suggest that when WWOX is Ser14 phosphorylated, it is potent in blocking nuclear bubbling and calcium influx.

Finally, antisera against Hyal-2 and pY216-Hyal-2 did not effectively block nuclear bubbling and calcium influx (Fig. 4e1-4). Membrane Hyal-2 acts as a cognate receptor for both TGF-β1 and hyaluronan to signal together with WWOX and Smad4 for exerting growth enhancement or suppression[13,29]. pY216-Hyal-2 antibody is potent in blocking cancer growth[24]. Intriguingly, p38 inhibitor SB203580 strongly suppressed both nuclear bubbling and calcium influx (Fig. 4f1).

Taken together, when HCT116 cells are exposed to UV, p53, WWOX and p38 participate in UV-mediated nuclear bubbling and calcium influx. In contrast, Hyal-2 and TβRI are not effective.

Ectopic WWOX restores calcium influx and nuclear bubbling in WWOXd cells in response to UV exposure

4T1 cancer cells were transiently overexpressed with an indicated WWOX construct using liposome-based Genefector and cultured for 48 hr. The cells were UV irradiated and then imaged by time-lapse microscopy at room temperature. The full-length WWOX restored calcium influx in 4T1 cells (Supplementary Fig. 5a; Supplementary Videos 10, 11). The first WW domain WW1 had a low activity in restoring calcium influx, and Y287F and Y61R mutants abolished the activity of endogenous WWOX (Supplementary Fig. 5a). 4T1 is a WWOXd cell line due to its failure in UV-mediated calcium influx[14]. At 200 μM, L-arginine failed to increase calcium influx and nuclear bubbling. L-arginine is needed for the synthesis of NO. In MDA-MB-231 cells, intracellular WWOX levels are fairly low[16]. Compared to other isoforms, WW1 was the most effective in restoring nuclear bubbling (or BCD) but failed to induce calcium influx (Supplementary Fig. 5b). Other indicated forms failed to restore calcium influx but enabled nuclear bubbling in MDA-MB-231 cells.

UV/cold shock induces global downregulation of cellular and housekeeping proteins

We examined whether UV/cold shock affects the protein expression in cells. COS7 cells were exposed to UV irradiation and subsequent incubation at 4°C for indicated times. Dramatic and rapid downregulation of house-keeping proteins α-tubulin and β-actin was observed (Fig. 5a; >70% for α-tubulin and >30% for β-actin). Cortactin, a protein involved in cell shape and migration[30], was downregulated rapidly in UV-irradiated COS7 cells (Fig. 5a; >90%). In response to UV/cold shock, the level of p53 was relatively unchanged (<10% reduction), whereas reduced p53 phosphorylation at S20 occurred in a time-related manner (Fig. 5a; >90% reduction in 2 hr).

Under similar conditions, L929S cells were exposed to UV and then cold shock, followed by incubation at specified temperatures and durations (Fig. 5b). UV/cold shock, or UV alone, drastically downregulated the expression of caspase 3, Bak and α-tubulin by greater than 90% in L929S cells at 4°C (Fig. 5b). Bcl-2, Bcl-x (Bcl-xL and Bcl-xS) and heat shock protein 70 (HSC70) were less affected (Fig. 5b; <10%). The reduction of caspase 3 may account for the failure of BCD-induced internucleosomal DNA fragmentation at room temperature or 4° C (Supplementary Fig. 2i-k). UV/cold shock-treated cells failed to migrate, which is mainly due to drastic loss of α-tubulin.

Relocation of α-tubulin and lamin B1 to the nucleus and bubble in UV/cold shock-treated L929S

By confocal microscopy, lamin B1 was shown to localize in the nuclear membrane, and α-tubulin in the cytoplasm of untreated L929S cells (Fig. 5c; top panel). When L929S cells were exposed to UV and cold shock, downregulation of α-tubulin was observed (Fig. 5c; bottom panel). Nuclear condensation occurred

and lamin B1 was still in the nuclear membrane (Fig. 5c; bottom panel). Shown in the Fig. 5d (left panel) is a merge of confocal sections for nucleus (DAPI), lamin B1 and α-tubulin. UV/cold shock-treated L929S cells exhibited relocation of α-tubulin to the nuclear bubble (Fig. 5d, right panel; red arrows). In certain confocal sections, bubbles contained α-tubulin and lamin B1, and DAPI (Fig. 5d, right panel; white arrow). We have reported that the inner membrane of the bubble is from the nucleus, and the outer membrane from the cell membranea[11,12]. In stark contrast, α-tubulin did not relocate to the bubbles (yellow arrows) of COS7 cells during BCD (Fig. 5e; yellow arrows).

Accumulating evidence shows that α-tubulin is associated with apoptosis[31,32]. We examined whether α-tubulin undergoes morphological changes caused by UV exposure and temperature alterations. COS7 cells were exposed to UV (480 mJ/cm^2), followed by culturing at 4 or 37°C for 90 min. The UV/cold shock-treated cells underwent BCD (Supplementary Fig. 6). Cold shock shrank the cells and reduced the cell sizes (Supplementary Fig. 6). UV rapidly decreased the expression of α-tubulin, whereas cold shock had no effect (Supplementary Fig. 5a). UV/cold shock-treated cells had reduced levels of α-tubulin, and part of the α-tubulin relocated to the nucleus (Supplementary Fig. 6). At 37°C, the UV-treated cells underwent apoptosis, and α-tubulin did not relocate to the nuclei (Supplementary Fig. 6).

UV and/or cold shock suppress RNA transcription and shuts down mRNA processing machinery

L929S cells were exposed to UV and/or cold shock, followed by purification of whole cell total RNA[20] and NanoDrop analysis for quality control (Fig. 6a). The concentration of total RNA was decreased by greater than 80% after UV irradiation. By reverse transcriptase-polymerase chain reaction (RT-PCR), mRNA expressions for p53, GAPDH, and β-actin were all dramatically decreased by greater than 95% after exposure to UV, cold shock, or UV/cold shock (Fig. 6a).

By gene chip analysis for mRNA expression profiling, we determined that downregulated genes are involved in mRNA processing and metabolic process and RNA splicing in L929S cells (Fig. 6b; Supplementary Fig. 7). Notably, upregulated genes included sensory perception of smell and chemical stimulus and G-protein coupled receptor protein signaling pathway (Fig. 6b-d). Specifically, microarray analysis showed that gene expression of glutathione peroxidase 2 (*Gpx2*) and eukaryotic translation initiation factor 2-alpha kinase 2 (*Eif2ak2*) were both increased after treated with UV/cold shock in L929S cells, respectively (Fig. 6c-d). By overlapping analysis, there are 12 upregulated genes and 4 downregulated genes (Fig. 6e). These regulated genes are: *Gpx2* codes for glutathione peroxidase 2; *Eif2ak2* for eukaryotic translation initiation factor 2-α kinase 2; *Bpifa5* for BPI Fold Containing Family A Member 1; *Ces3b* for Carboxylesterase 3; *Mir139* for MicroRNA 139; *Olfr12* for Olfactory Receptor Family 5 Subfamily S Member 1 Pseudogene; *Rps15* for Ribosomal Protein S15; *Tcrb-J* for T cell receptor β joining region; *mt-Tm* for Mitochondrially Encoded TRNA-Met (AUA/G). *Gm10736*, *Gm11353*, and *Gm6613* do not code for proteins. Among the downregulated genes, *Mbtps2* codes for Membrane Bound Transcription Factor Peptidase, and *Sept7* for CDC10 Protein Homolog. *Gm5446* and *Gm5792* do not code for proteins.

UV and cold shock together rapidly suppress protein expression from skin to liver in the hairless mice

We investigated the effect of UV/cold shock in regulating protein expression in hairless mice[33]. Hairless mice were subjected to whole-body UV irradiation (960 mJ/cm^2) and then subjected to temperature shock at -30° or 37° C for indicated times. Mice were then sacrificed. In the mouse skin, UV had little or no effect on the expression of β-actin, GPX1/2[34], PKR (protein kinase R; encoded by *Eif2ak2* gene)[35], α-tubulin, and TRAF2[11,12], but significantly upregulated the expression of WWOX (Fig. 7a-d; Supplementary Fig. 8a-l). Of particular interest is that UV upregulated WWOX phosphorylation at Ser14 (pS14-WWOX) by one-fold (Fig. 8k-l). pS14-WWOX enhances the progression of cancer and Alzheimer's disease[36−39]. During cold shock of the animals at -30°C for 20 min, upregulation of the aforementioned proteins occurred (Fig. 7a-d; Supplementary Fig. 8a-l). However, the protein levels were significantly reduced when the mice were under cold shock for 40 min. When the mice were exposed to UV and then cold shock for 20 or 40 min, dramatic downregulation of the aforementioned proteins occurred. However, when UV-treated mice were kept at 37 C for 20 min, majority of protein expression remained largely unchanged, except that pS14-WWOX was significantly upregulated (Fig. 7a-d; Supplementary Fig. 8a-l).

In the mouse liver, UV rapidly suppressed the expression of β-actin (Fig. 7e-f), TRAF2 (Supplementary Fig. 9a), p53 and pS20-p53 (Supplementary Fig. 9f-g), and Bcl-x (Supplementary Fig. 9h). However, UV alone had no effect on the expression of GPX1/2 (Fig. 7g), PKR (Fig. 7h; Supplementary Fig. 9b), and WWOX and pS14-WWOX (Supplementary Fig. 9c, d) in the liver. In contrast, UV, cold shock, or UV/cold shock reduced the expression of pY33-WWOX in the liver (Supplementary Fig. 9e). When mice were exposed to cold shock (-30°C) for 30 min and then kept at 37° C for indicated times, significant downregulation of the aforementioned proteins were observed in the mouse liver (Fig. 7; Supplementary Fig. 9). pY33-WWOX was significantly increased in the liver post treatment with UV and 37° C for 15 min, followed by reduction in the next 15 min (Supplementary Fig. 9). Significant upregulation of pY33-WWOX in organs at 37° C is probably needed to exert apoptosis *in vivo*[20−25, 40]. Additionally, downregulation of p53, pS20-p53, and Bclx occurred when mice were subjected to UV and/or cold shock or exposure to 37° C (Supplementary Fig. 9f-h).

Collectively, when hairless mice were UV irradiated and cold-shocked, dramatic protein downregulation occurred in the skin. The signal was then transmitted to the liver to cause protein downregulation. The event may account for the pathologies found in patients with frostbite.

UV/cold shock induces nuclear accumulation of TRAF2/WWOX complex to regulate bubbling

We reported that antiapoptotic TRAF2 is dramatically downregulated during frostbite in human skin, and that TRAF2 counteracts with the function of WWOX and p53 in inducing BCD[11,12]. Here, we further elucidate the functional interactions between TRAF2 and WWOX during BCD. When L929S cells were exposed to UV (480 mJoule/cm^2) and then cold shock at 4°C for 15 min to 4 hr, expression of WWOX, TRAF2 and α-tubulin was downregulated by greater than 50% (Fig. 8a). Cold shock alone did not affect

the expression of WWOX, TRAF2 and α-tubulin (Fig. 8a). pY33-WWOX levels were not reduced. Cold shock or UV/cold shock gradually reduced p53 expression (Fig. 8a).

An EGFP-TRAF2(124-233) construct was made for transient expression of the zinc finger domain in TRAF2. We established stable transfectants of L929S cells for expressing EGFP-TRAF2(124-233), ECFP-TRAF2, ECGP, or EGFP (Fig. 8b). EGFP-TRAF2(124-233) strongly suppressed UV/cold shock-induced BCD. The full-length ECFP-TRAF2 was not expressed and did not exhibit an inhibitory activity (Fig. 8b). Similar results were observed for the suppression of BCD when COS7 cells were stably transfected with EGFP-TRAF2(124-233) and L929S with ECFP-TRAF2 (Fig. 8c-d).

By Cytotrap yeast two-hybrid analysis[13,20-22], we determined the positive binding of full-length WWOX with full-length TRAF2 (Fig. 8e). In positive controls, p53 physically bound WWOX and MafB underwent self-association (Fig. 8e). Additionally, we carried out Förster resonance energy transfer (FRET) microscopy[13,29,40-42]. There was an increased binding of EGFP-TRAF2 with DsRedM (monomeric DsRed)-WWOX in UV/cold shock-treated COS7 cells at 37°C (Fig. 8f). At low temperature (4°C), the EGFP-TRAF2/DsRedM-WWOX complex became dissociated in 60 min (Fig. 8f). By fluorescent immunostaining, UV/cold shock induced nuclear co-localization of endogenous WWOX with TRAF2 in COS7 cells (Fig. 8g). In the absence of WWOX, endogenous TRAF2 in $Wwox^{-/-}$ knockout MEF cells did not relocate to the nucleus in response to UV/cold shock (Fig. 8h), suggesting that TRAF2 requires WWOX to co-translocate to the nucleus.

By co-immunoprecipitation, UV/cold shock induced the dissociation of the endogenous WWOX/TRAF2 complex in 30 min in COS7 cells (Fig. 8i). TRADD, a TNF receptor adaptor protein[43], physically bound TRAF2 without dissociation during the course of UV/cold shock (Fig. 8i). Dissociation of the TRAF2/WWOX complex correlates with WWOX dephosphorylation at Y287. pY287-WWOX is subjected to ubiquitination and proteasomal degradation[44]. In the absence of WWOX, UV/cold shock failed to induce translocation of cytosolic TRAF2 to the nucleus in the knockout $Wwox^{-/-}$ MEF cells (Fig. 8J). However, p53 underwent nuclear translocation (Fig. 8j). Overall, the zinc finger domain of TRAF2 blocked the function of WWOX in inducing BCD at room temperature. Both WWOX and TRAF2 form complex to relocate to the nucleus. Conceivably, dissociation of the complex at low temperature facilitates WWOX function in inducing NO production.

Discussion

This study concerns UV/cold shock-mediated frostbite in humans and animals. The disastrous event may accidentally occur in the polar regions or outer space. Our supporting data show that UV/cold shock rapidly shut down the global gene transcription and protein synthesis machinery both in cells and hairless mice. Also, the WWOX/p53/TRAF2 signaling pathway is activated to control BCD. Nuclear translocation of TRAF2 requires WWOX. We reported that nuclear translocation of WWOX requires a trafficking protein TRAPPC6A[39,45,46]. Whether TRAPPC6A is recruited in the WWOX/p53/TRAF2 signaling complex remains to be established. In hairless mice, UV/cold shock causes protein downregulation in the

skin and then the signal rapidly goes to the liver. Conceivably, the sequential event causes serious damages to their skin and internal organs, and eventually results in limb amputations, organ failure and death[47].

We demonstrated the crucial role of WWOX in regulating BCD in WWOXf cells in response to UV or UV/cold shock at room temperature. In most cases, each nucleus generates a single bubble. The nuclear bubble possesses an inner nuclear membrane and an outer cytoplasmic membrane[11,12]. NO gas in the bubble is probably mixed in the cytoplasmic liquid[11,12]. The bubble can be detached from the cell and released to the extracellular surface, or it continues to stay on the cell surface. In the absence of calcium, the bubble may shrink and disappear. In contrast, UV/cold shock induces WWOXd cells to undergo nuclear explosion and death. Compared to WWOXf, UV does not raise the levels of NO gas in WWOXd cells. How WWOXd cells explode in response to UV remains to be established. Ectopically expressed full-length WWOX in WWOXd breast 4T1 and MDA-MB-231 cells allows restoration of nuclear bubbling. Interestingly, calcium influx is restored in 4T1 cells, but not in MDA-MB-231 cells. The mechanism of this regard remains to be elucidated. In our recent report[14], we have deposited 27 videos regarding BCD, POD and calcium influx from WWOXf and WWOXd cells (see https://doi.org/10.6084/m9.figshare.14560782).

As determined by time-lapse microscopy, WWOXf cells rapidly exhibit the following sequential molecular events after UV and/or cold shock exposure: 1) loss of mitochondrial membrane potential, 2) upregulation of NO and release of nucleolar content for nuclear bubbling, 3) induction of calcium influx, 4) failure in excluding trypan blue with time, 5) reduction in calcein retention with time, and 7) final uptake of PI, indicative of cell death. In contrast to WWOXf, WWOXd cells do not show efficient production of NO and processing calcium influx, but exhibit a strong expression of stress fiber when cells are reaching a status of death. In contrast, UV-mediated stress fiber formation for WWOXf cells is poor. ATP and NTP uptakes are altered in control and UV/cold shock-treated WWOXf and WWOXd cells. The extent of stemness in the spheres of breat 4T1 cells is strong, compared to cells in the surrounding areas. UV irradiation suppresses the stemness. Thus, loss of WWOX or functional alterations of WWOX allows WWOXd cancer cells to exhibit aberrant behaviors, including accelerated migration, loss of recognition by wild type parental cells, and attacking parental cells from a distance[14]. While WWOXd cells are mainly malignant cancer cells, their presence in the solid tumors is hard to dectect. Based upon our finding, we may be able to detect the presence of WWOXd cells due to their low retention of calcein and increased stress fiber formation under environmental impact (e.g. chemotherapeutic drugs).

Intracellular p53 and WWOX are involved in UV-mediated nuclear bubbling and calcium influx in WWOXf cells. In addition, SB203580 completely inhibits calcium influx, suggesting that p38 is involved. WWOX and p53 are known binding partners in apoptosis and BCD[17–20]. Whether they complex with p38 is unknown. During BCD, there is an initial increase followed by reduction in calcium influx in UV and UV/cold shock-treated WWOXf cells.

Among WWOX-binding partners[20–25,28,29,36–42], we have examined p53, TβRII and Hyal-2 in calcium influx and nuclear bubbling in WWOXf HCT116 cells. Wild type p53 participates in calcium influx but not in

nuclear bubbling in UV-treated HCT116 cells. In contrast, isoforms p53β or p53γ antibody retards the nuclear bubbling but cannot affect calcium influx. TβRI and TβRII do not play a role in both calcium influx and nuclear bubbling.

WWOX is involved in nuclear bubbling and calcium influx. Polyclonal antibodies against WWOX at amino acid 7-21, 28-42 and 286-299, respectively, suppress calcium influx, whereas these antibodies do not retard the timing of the initiation of nuclear bubbling. In parallel, antibodies against pY33-, pT12- and pS14-WWOX strongly inhibit calcium influx. Importantly, pT12- and pS14-WWOX antibodies strongly retard the nuclear bubbling. Finally, we determined that ectopic WWOX restores calcium influx and nuclear bubbling in 4T1 breast cancer cells in response to UV exposure, but only nuclear bubbling in UV-treated MDA-MB-231 cells. The first WW domain of WWOX is responsible for both events. Taken together, p53, WWOX and p38 participate in UV-mediated nuclear bubbling and calcium influx in HCT116 cells. How these proteins collaborate with each other in causing nuclear bubbling and calcium influx remains to be established.

In response to UV/cold shock, rapid shutdown of the machinery for RNA and protein synthesis occurs in cells, which leads to irreversible BCD. By gene chip analysis, we determined that gene expression of *Gpx2* and *Eif2ak2*, respectively, encoding GPX and PKR proteins[34,35], is affected in L929S cells. In parallel experiments, UV/cold shock-treated hairless mice exhibit rapid downregulation of GPX1/2, PKR and many other proteins. How GPX1/2 and PKR contribute to BCD and frostbite is unknown and will be established. Overall, how downregulated proteins contribute to the severity of frostbite remains to be established. For example, pS14-WWOX enhances the progression of cancer and Alzheimer's disease[32–35]. UV/Cold shock also reduces pS14-WWOX. Its functional significance in damage by frostbite is unknown.

Methods

Cell lines and cDNA constructs. Cell lines used in this study were: 1) African Green Monkey SV40-tranfected kidney COS7 fibroblasts[14], 2) mouse TNF sensitive L929S fibrosarcoma cells[14], 3) mouse TNF resistant L929R fibrosarcoma cells[14], 4) mouse 4T1 mammary carcinoma cells[14], 5) human breast MCF7 adenocarcinoma cells[14], SCC9 and SCC15[14], 6) human lung cancer H441, H661, PC9 and H1299 (from ATCC and kind gifts of the core facility of the National Cheng Kung University Hospital), 7) human colon cancer HCT116, and 8) human breast MDA-MB-231 adenocarcinoma cell lines, which are MDA-MB-231[14], and MDA-MB-231 (NHRI) and MDA-MB-231 (IV2-3) (from the National Health Research Institute, Taiwan). All cell lines were maintained in DMEM medium (Thermo) containing 10% heat-inactivated fetal bovine serum (FBS) (Gibco), except that L929S and L929R were maintained in RPMI-1640 medium (Sigma) containing 10% heat-inactivated FBS. Cells were incubated at 37°C with 5% humidified CO_2 atmosphere. Mouse WWOX cDNA expression constructs were made: 1) WWOX-pECFPC1, 2) WW1- pECFPC1, 3) WW2-pECFPC1, 4) dn-WWOX-pECFPC1, 5) WWOX(Y61R)-pECFPC1, and 6) WWOX(Y287F)-pECFPC1[22,41].

Time-lapse bright field and fluorescent microscopy and time-lapse holography. A UV crosslinker (FB-UVXL-1000), emitting UVC at 265 nm, was used to irradiate cells at an indicated setting, e.g. 960

mJoule/cm^2 (Fisher Scientific)[11]. Post exposure, cells were subjected to cold shock at 4 or 10°C for indicated times. The number of cells undergoing BCD or POD were counted by an inverted microscope (Olympus). Also, time-lapse bright field and fluorescent microscopy (Nikon Eclipse TE2000-U) were carried out to image BCD or POD[14,42]. Further, UV/cold shock-treated cells were imaged by time-lapse holographic microscopy (HoloMonitor M4) and analyzed by Hstudio M4 Tracking software.

Trypan blue exclusion for cell viability. Cells were stained with trypan blue to determine the extent of cell viability. Live cells exclude the trypan blue dye, whereas dead cells retain the dye. Cells in Petri dishes were washed with 1X phosphate buffered saline (PBS) for 1 time, and then incubated with 0.2% trypan blue in 1X PBS for 2 min, followed by descanting the dye and counting the number of total cells and trypan blue-positive cells.

MTT assay for cell viability. MTT assay was used to measure functionally active metabolism in live cells[20−22]. Cells were seeded on 96-well plates overnight and then added MTT ((3-(4,5-dimethylthiazol-2-yl)-2,5-diphenyltetrazolium bromide; 0.5 mg/ml; Protech) for incubation at 37°C for 4 hours, followed by descanting the culture supernatants and adding 100 μl DMSO to dissolve the MTT-derived formazan purple crystals. Absorbance was measured using SpectraMax M3 (Molecular Devices) at a wavelength of 570 nm.

Internucleosomal DNA fragmentation. Chromosomal DNA fragmentation assay was carried out[6]. Post UV/cold shock, cells were harvested and lysed with 50 μl lysis buffer (1% NP-40 in 20 mM EDTA, 50 mM Tris-HCl, and pH 7.5) for 10 sec. These samples were centrifuged (1600 g, 5 min), and supernatants harvested. This step was repeated once. The supernatants were added 1% SDS and RNase A (5 μg/μl) for incubation for 2 hours at 56°C, and then treated with proteinase K (2.5 μg/μl) overnight at 37°C. After adding 1/2 volume of 10 M ammonium acetate, DNA preparations were precipitated with 2.5 volumes of ethanol, resuspended in double-distilled H$_2$O, and analyzed by 1.5% agarose gel electrophoresis.

Western Blotting. Cells were lysed with a lysis buffer (1% SDS, 0.5% NP-40, 0.1% Triton X-100) in the presence of 7 μl of a protease inhibitor cocktail (Sigma) plus 1 mM PMSF and 1 mM Na$_3$VO$_4$, and incubated on ice for 30 min. The lysates were centrifuged at 4°C at 13200 rpm for 15 min (Eppendorf microfuge) and then processed for standard SDS-PAGE and immunoblotting[20−25].

Immunofluorescence staining

Cells were cultured on cover slips overnight or up to 48 hr. After indicated experiments, cells were fixed with 3.7% paraformaldehyde for 20 min at room temperature and permeabilized with 0.5% Triton X-100 in 3.7% paraformaldehyde for another 10 min[13,28,41]. Cells were washed 3 times with 1X phosphate-buffered saline (PBS) and added with 4% BSA for overnight incubation at 4°C to block non-specific binding sites. Primary antibodies (in 4% BSA) were added to the cells for 2 hr at room temperature, or 3 to 6 hr at 4°C, for antigen detection. Cell were washed 3 times with 1X PBS and then stained for 1 hr with fluorescent secondary antibodies, conjugated with red fluorescent rhodamine, Texas red, or Alexa 555

(Molecular Probes/Invitrogen or Jackson Laboratory). For dual color staining, another secondary antibodies were conjugated with green fluorescent Alexa Fluor 488 or Fluorescein (Molecular Probes/Invitrogen or Jackson Laboratory), and counter-stained with DAPI for nuclei for 2 min. Confocal or immunofluorescence microscopy was then carried out.

Measuring BCD, calcium influx and others by fluorescence time-lapse microscopy

Live WWOXf or WWOXd cells were cultured overnight. The cells were added an aliquot of Fluo-8 (50 μM) and nontoxic levels of PI (2 μg/ml) and DAPI (10 μg/ml), exposed to UV irradiation (240–960 mJoule/cm^2) and/or cold shock for 5 to 10 min, and then subjected to time-lapse microscopy at room temperature at 200x magnification to image calcium influx and BCD[14]. One picture was taken per 2 min. Additional fluorescent probes used were: 1) MitoTracker Red or Green CMXRos for measuring mitochondrial membrane potential in live cells (Molecular Probes/Invitrogen); 2) Calcein Green, AM for measuring cell viability (Invitrogen); 3) 2',7'-Dichlorofluorescin diacetate (DCF) for measuring ROS production (Sigma-Aldrich); 4) 4-Amino-5-Methylamino-2',7'-Difluorofluorescein Diacetate (DAF-fm) for measuring NO production (ThermoFisher); 5) Phalloidin green or red for measuring stress fiber formation (Santa Cruz Biotechnology); 6) BioTracker ATP-Red Live Cell Dye for measuring NTP (Merck); 7) BioTracker NTP-Transporter Molecule for measuring NTP (Merck); 8) BioTracker 529 Green Pluripotent Stem Cell Dye for measuring cell stemness (Merck).

RNA isolation and gene expression profiling by DNA chip microarray

Where indicated, L929S cells were exposed to UV/cold shock and then washed once with 1X PBS. The cells were lysed with Trizol reagent, and the solution added one-tenth volume of chloroform followed by incubation on ice for 15 min[20,21]. Following centrifugation at 13000 rpm for 15 min, the top layer of solution was harvested and precipitated with 2 volumes of isopropanol at -20°C for 1 hr or up to overnight. Again, samples were centrifuged (13000 rpm, 15 min). RNA pellets were washed 4 times with 100% ethanol. The RNA pellet was resuspended in DEPC water and analyzed by RNA gel electrophoresis and NanoDrop (ND-1000). The RNA was transcribed to cDNA by reverse transcription and polymerase chain reaction (RT/PCR). Six gene microarray chips (Affymetrix) were hybridized with the amplified cDNA, according to the manufactural manual.

Hairless mice subjected to UV/cold shock treatment

All experiments involved in animal use by Chang and Sheu laboratories have been approved by the Institutional Animal Care and Use Committee (IACUC) of the National Cheng Kung University College of Medicine. Hairless mice received whole-body UV irradiation (960 mJoule/cm^2) and/or temperature-shock at -30º or 37º C for indicated times. In controls, mice received nothing. After experiments, mice were sacrificed. Organs were harvested and fixed with 0.4% paraformaldehyde. Tissue sections were made for immunohistochemistry using specific antibodies.

Quantification and statistics analysis

Where indicated, data were analyzed by one-way Anova and Student's *t* test using Microsoft Excel and Prism 7. Data were expressed as mean ± standard deviation. $p < 0.05$ was considered as statistically significant.

Declarations

Author contributions: (a) Research: (1) Animal experiments: C-C T, H-M S; (2) Immunohistochemistry: W-T D; (3) Western blots: C-C T, S-J C, N-S C; (4) Cell lines and experiments: C-C T, S-J C, W-T D, S-N W, L-H W, N-S C; (5) Time-lapse microscopy: C-C T, N-S C; (6) Gene chip analysis: T-Y L, K-T L, L-J S; (7) cDNA clones: M-H L, S-R L; (8) Manuscript writing: C-C T, N-S C; (9) Antibody production: T-Y L, K-T L, M-H L, S-R L, N-S C; (10) Conceived ideas, designed peptides, carried out time-lapse fluorescent microscopy, analyzed data, grant writing, and wrote the manuscript: N-S C. **(b) Data**: (1) Figures 1, 2, 5, 6, and Supplementary Figures 1, 2, 6 and Video 3-9: C-C T; (2) Figures 3, 4, and Supplementary Figures 3, 4, 5, Table 1, and Videos 1, 2, 10-13: N-S C; (3) Figure 7, and Supplementary Figures S8, S9: W-T D; (4) Figure 8: S-J C and C-C T; (5) Figure S7: C-C T and L-J S; (6) graphic arts: Y-A C. All authors have read and agreed to the published version of the manuscript.

Competing interests: The authors declare no competing interests.

References

1. Edinger, A.L., Thompson, C.B. Death by design: apoptosis, necrosis and autophagy. *Curr Opin Cell Biol.* **16**, 663–669 (2004).

2. Galluzzi, L. et al. Molecular definitions of cell death subroutines: recommendations of the Nomenclature Committee on Cell Death 2012. *Cell Death Differ.* **19**, 107–120 (2012).

3. Gómez-Suaga, P., Bravo-San Pedro, J.M., González-Polo R.A., Fuentes J.M., Niso-Santano M. ER–mitochondria signaling in Parkinson's disease. *Cell Death Dis.* **9**, 1–12 (2018).

4. Wojton, J., Meisen W.H., Kaur B. How to train glioma cells to die: molecular challenges in cell death. *J Neurooncol.* **126**, 377–384 (2016).

5. Negroni, A., Cucchiara, S., Stronati, L. Apoptosis, necrosis, and necroptosis in the gut and intestinal homeostasis. *Mediators Inflamm.* (2015).

6. Lin, H.P. et al. Identification of an in vivo MEK/WOX1 complex as a master switch for apoptosis in T cell leukemia. *Genes Cancer.* **2**, 550–562 (2011).

7. Tsai, C. et al. WWOX suppresses autophagy for inducing apoptosis in methotrexate-treated human squamous cell carcinoma. *Cell Death Dis.* **4**, e792-e792 (2013).

8. Mora, R., Régnier-Vigouroux, A. Autophagy-driven cell fate decision maker: activated microglia induce specific death of glioma cells by a blockade of basal autophagic flux and secondary apoptosis/necrosis. *Autophagy.* **5**, 419–421 (2009).

9. Proskuryakov, S.Y., Konoplyannikov, A.G., Gabai, V.L. Necrosis: a specific form of programmed cell death? *Exp Cell Res.* **283**, 1–16 (2003).

10. Fink, S.L., Cookson, B.T. Apoptosis, pyroptosis, and necrosis: mechanistic description of dead and dying eukaryotic cells. *Infect Immun.* **73**, 1907–1916 (2005).

11. Chen, S.J. et al. UV irradiation/cold shock-mediated apoptosis is switched to bubbling cell death at low temperatures. *Oncotarget.* **6**, 8007 (2015).

12. Chang, N.S. Bubbling cell death: A hot air balloon released from the nucleus in the cold. *Exp Biol Med (Maywood).* **241**, 1306–1315 (2016).

13. Hsu, L.J. et al. Hyaluronan activates Hyal-2/WWOX/Smad4 signaling and causes bubbling cell death when the signaling complex is overexpressed. *Oncotarget.* **8**, 19137 (2017).

14. Chen, Y.A. et al. Normal cells repel WWOX-negative or-dysfunctional cancer cells via WWOX cell surface epitope 286-299. *Commun Biol.* **4**, 1–19 (2021).

15. Chou, P.Y. et al. Strategies by which WWOX-deficient metastatic cancer cells utilize to survive via dodging, compromising, and causing damage to WWOX-positive normal microenvironment. *Cell Death Discov.* **5**, 97 (2019).

16. Chang, N.S. et al. 17 β-Estradiol upregulates and activates WOX1/WWOXv1 and WOX2/WWOXv2 in vitro: potential role in cancerous progression of breast and prostate to a premetastatic state in vivo. *Oncogene.* **24**, 714–723 (2005).

17. Kawarski, M., Hagerman, T.K., Karver, C.E. Lazaroids U83836E and U74389G are potent, time-dependent inhibitors of caspase-1. *Chem Biol Drug Des.* **86**, 1049–1054 (2015).

18. Hill, R.L., Singh, I.N., Brelsfoard, J., Hall, E.D. Pharmacological inhibition of lipid peroxidative damage by the 21-aminosteroid U-74389G improves cortical mitochondrial function following traumatic brain injury in young adult male rats. *Neuropharmacology.* **170**, 108023 (2020).

19. Marquet, P., Depeursinge, C., Magistretti, P.J. Review of quantitative phase-digital holographic microscopy: promising novel imaging technique to resolve neuronal network activity and identify cellular biomarkers of psychiatric disorders. *Neurophotonics.* **1**, 020901 (2014).

20. Chang, N.S. et al. Hyaluronidase induction of a WW domain-containing oxidoreductase that enhances tumor necrosis factor cytotoxicity. *J Biol Chem.* **276**, 3361–3370 (2001).

21. Chang, N.S., Doherty, J, Ensign, A. JNK1 physically interacts with WW domain-containing oxidoreductase (WOX1) and inhibits WOX1-mediated apoptosis. *J Biol Chem.* **278**, 9195–9202 (2003).

22. Chang, N.S. et al. WOX1 is essential for tumor necrosis factor-, UV light-, staurosporine-, and p53-mediated cell death, and its tyrosine 33-phosphorylated form binds and stabilizes serine 46-phosphorylated p53. *J Biol Chem.* **280**, 43100–43108 (2005).

23. Chang, N.S., Hsu, L.J., Lin, Y.S., Lai, F.J., Sheu, H.M. WW domain-containing oxidoreductase: a candidate tumor suppressor. *Trends Mol Med.* **13**, 12–22 (2007).

24. Su, W.P. et al. Therapeutic Zfra4-10 or WWOX7-21 peptide induces complex formation of WWOX with selective protein targets in organs that leads to cancer suppression and spleen cytotoxic memory Z Cell activation in vivo. *Cancers (Basel).* **12**, 2189 (2020).

25. Wang, W.J. et al. WWOX possesses N-terminal cell surface-exposed epitopes WWOX7-21 and WWOX7-11 for signaling cancer growth suppression and prevention in vivo. *Cancers (Basel).* **11**, 1818 (2019).

26. Bourdon J.C. p53 and its isoforms in cancer. *Br J Cancer.* **97**, 277–282 (2007).

27. Vieler, M., Sanyal, S. p53 isoforms and their implications in cancer. *Cancers (Basel).***10**, 288 (2018).

28. Hsu, L.J. et al. Transforming growth factor β1 signaling via interaction with cell surface Hyal-2 and recruitment of WWOX/WOX1. *J Biol Chem.* **284**, 16049–16059 (2009).

29. Huang, S.S. et al. Chang N.S. Role of WW domain-containing oxidoreductase WWOX in driving T cell acute lymphoblastic leukemia maturation. *J Biol Chem.* **291**, 17319–17331 (2016).

30. Schnoor, M., Stradal, T.E., Rottner, K. Cortactin: cell functions of a multifaceted actin-binding protein. *Trends Cell Biol.* **28**, 79–98 (2018).

31. Wang, Q., Liu, X. The dual functions of α-tubulin acetylation in cellular apoptosis and autophage induced by tanespimycin in lung cancer cells. *Cancer Cell Int.* **20**, 1–10 (2020).

32. Kamal, M.A. et al. Tubulin Proteins in Cancer Resistance: A Review. *Curr Drug Metab.* **21**, 178–185 (2020).

33. Wu, C.H. et al. Solanum incanum extract (SR-T100) induces human cutaneous squamous cell carcinoma apoptosis through modulating tumor necrosis factor receptor signaling pathway. *J Dermatol Sci.* **63**, 83–92 (2011).

34. Brigelius-Flohé, R. Glutathione peroxidases and redox-regulated transcription factors. *Biol Chem.* **387**, 1329–35 (2006).

35. Lee, K.S. et al. Inhibition of UVB-Induced inflammation by Laminaria japonica extract via regulation of nc886-PKR pathway. *Nutrients.* **12**, 1958 (2020).

36. Hsu, C.Y. et al. WWOX and Its Binding Proteins in Neurodegeneration. *Cells.* **10**, 1781 (2021).

37. Liu, C.C. et al. WWOX Phosphorylation, Signaling, and Role in Neurodegeneration. *Front Neurosci.* **12**, 563 (2018).

38. Huang, S.S., Chang, N.S. Phosphorylation/de-phosphorylation in specific sites of tumor suppressor WWOX and control of distinct biological events. *Exp Biol Med (Maywood).* **243**, 137–147 (2018).

39. Lee, M.H. et al. Zfra restores memory deficits in Alzheimer's disease triple-transgenic mice by blocking aggregation of TRAPPC6AΔ, SH3GLB2, tau, and amyloid β, and inflammatory NF-κB

activation. *Alzheimers Dement (N Y)*. 3, 189–204 (2017).

40. Chou, P.Y. et al. A p53/TIAF1/WWOX triad exerts cancer suppression but may cause brain protein aggregation due to p53/WWOX functional antagonism. *Cell Commun Signal.* **17**, 1–16 (2019).

41. Li, M.Y. et al. Dramatic co-activation of WWOX/WOX1 with CREB and NF-κB in delayed loss of small dorsal root ganglion neurons upon sciatic nerve transection in rats. *PLoS One*. **4**, e7820 (2009).

42. Kuo, H.L., Ho, P.C., Huang, S.S., Chang, N.S. Chasing the signaling run by tri-molecular time-lapse FRET microscopy. *Cell Death Discov*. **4**, 1–9 (2018).

43. Li, Z., Yuan, W., Lin, Z. Functional roles in cell signaling of adaptor protein TRADD from a structural perspective. *Comput Struct Biotechnol J*. **18**, 2867–2876 (2020).

44. Mahajan, N.P, Whang, Y.E., Mohler, J.L., Earp, H.S. Activated tyrosine kinase Ack1 promotes prostate tumorigenesis: role of Ack1 in polyubiquitination of tumor suppressor Wwox. *Cancer Res.* **65**, 10514–10523 (2005).

45. Chang, J.Y. et al. Trafficking protein particle complex 6A delta (TRAPPC6AΔ) is an extracellular plaque-forming protein in the brain. *Oncotarget*. **6**, 3578–3589 (2015).

46. Chang, J.Y., Chang, N.S. WWOX dysfunction induces sequential aggregation of TRAPPC6AΔ, TIAF1, tau and amyloid β, and causes apoptosis. *Cell Death Discov*. **1**, 15003 (2015).

47. Regli, I.B., Strapazzon, G., Falla, M., Oberhammer, R., Brugger, H. Long-Term Sequelae of Frostbite-A Scoping Review. *Int J Environ Res Public Health*. **18**, 9655 (2021).
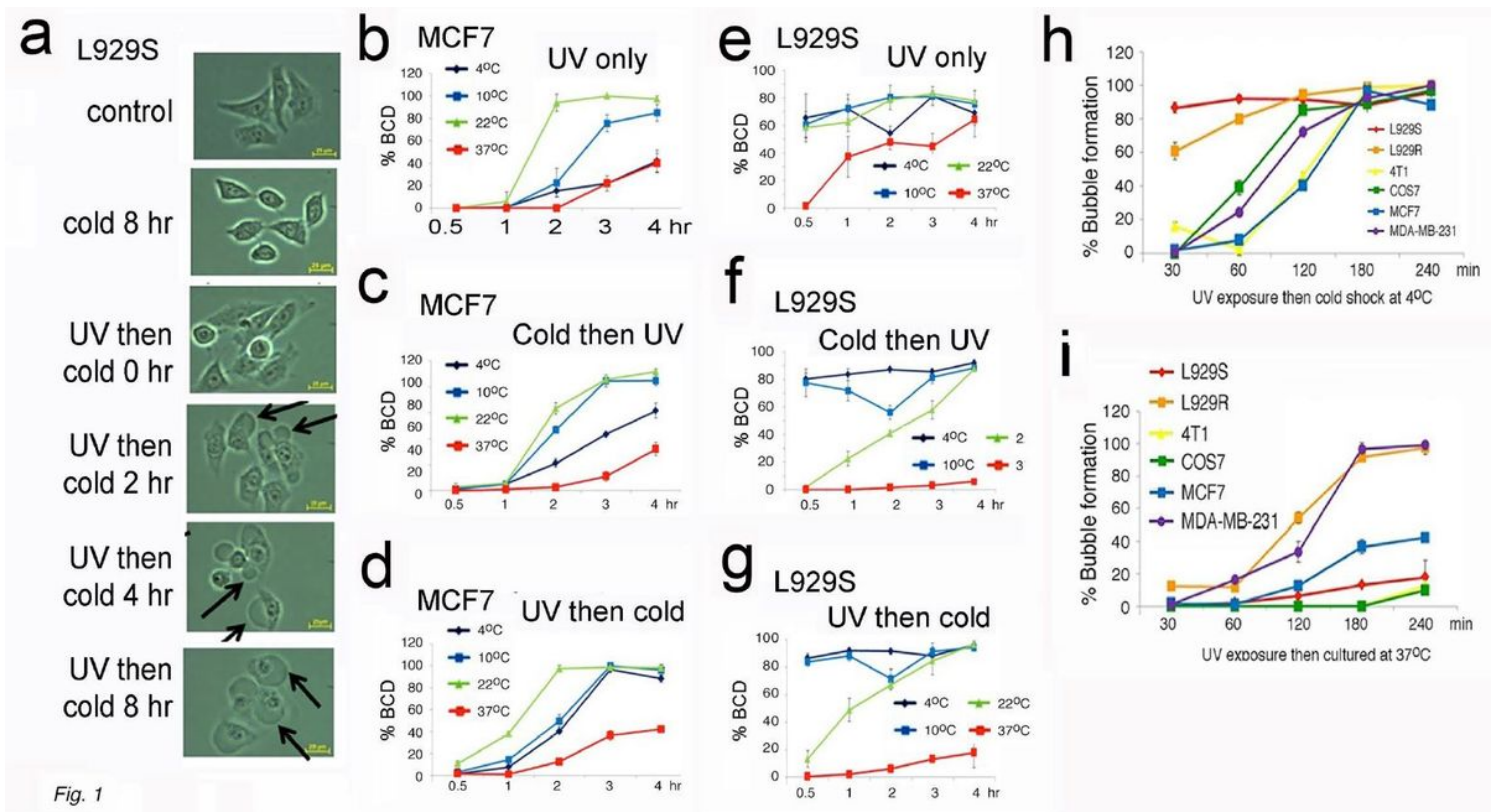
Figures

Fig. 1

Figure 1

UV/Cold shock induces BCD or POD in cell lines. a WWOXf L929S fibroblasts were exposed to UV irradiation (480 mJoule/cm2) and then cold shock at 4oC for indicated times. Bubbles were indicated by black arrows. In controls, cells were without treatment or subjected to cold shock for 8 hr. b−d WWOXf breast MCF7 cells were exposed to UV irradiation (480 mJ/cm2) only (b), cold shock at 4oC for 5 min and then UV irradiation (480 mJ/cm2) (c), or UV irradiation (480 mJ/cm2) and then cold shock at 4oC for 5 min (d). The cells were then incubated at indicated temperatures for various durations, followed by measuring bubble formation (mean ± standard deviation; n=3). e-g Under similar conditions, L929S cells were subjected to identical treatments. h−j WWOXd breast MDA-MB-231 cells (j) and two variants (h,i) were subjected to cold shock at 4oC for 5 min and then UV irradiation (480 mJ/cm2), follwed by culturing at indicated temperatures for various times (mean ± standard deviation; n=3). MDA-MB-231 cells were from our laboratory, and MDA-MB-231(NH) and MDA-MB-231(IV-2-3) from the National Health Research Institute, Taiwan. MDA-MB-231(IV-2-3) is a metastatic line.
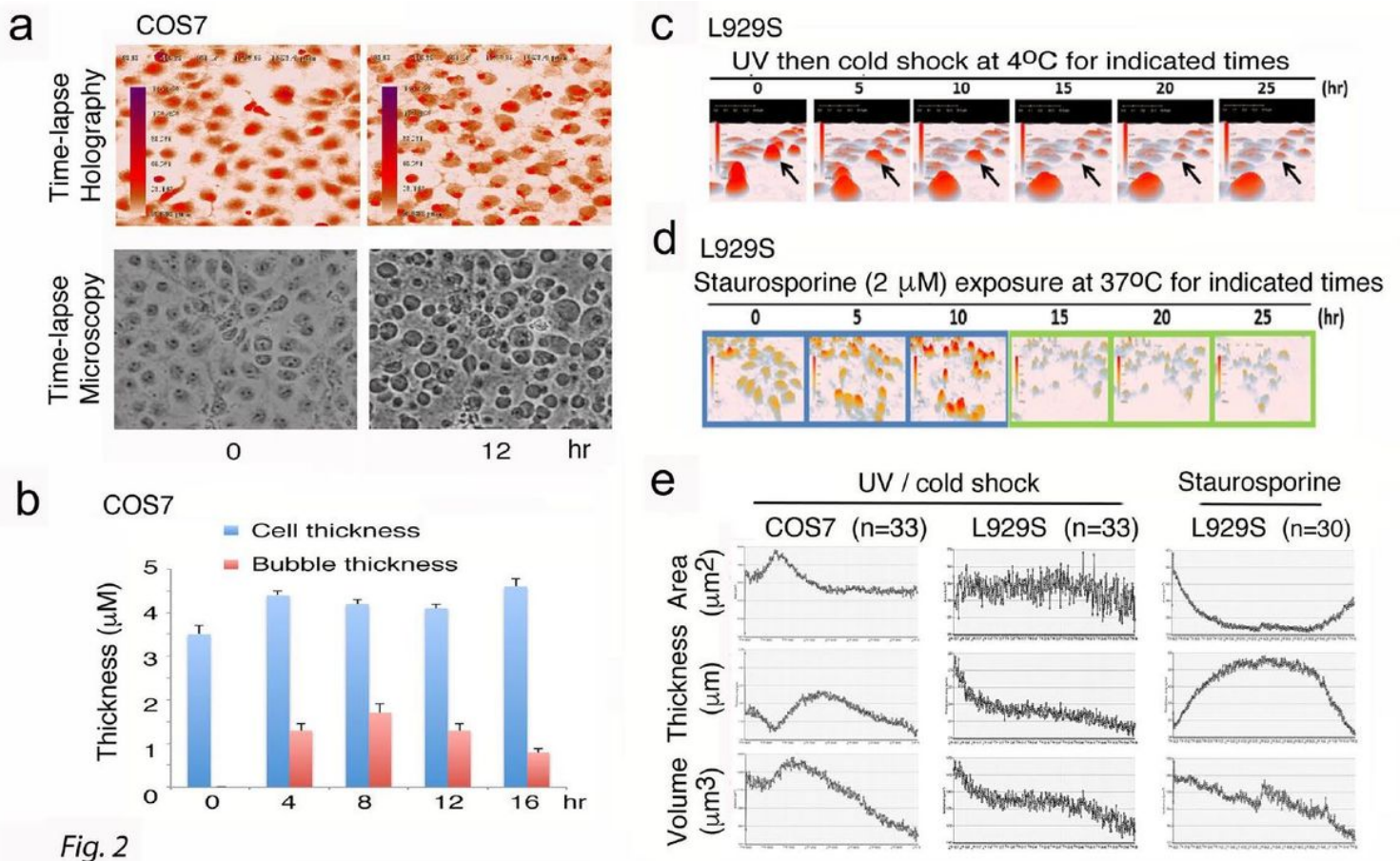

Fig. 2

Figure 2

Time-lapse holographic microscopy shows dramatically increases cell thickness during apoptosis, but not BCD. a, b COS7 cells were exposed to UV and then cold shock at 4oC for 12 hr. Cell bubbles were observed, as determined by light and holographic microscopy, respectively. The COS7 cell thickness is approximately 4.5 µm, and the bubble thickness less than 2 µm. c Under similar conditions, time-related

bubbling is shown at 4oC in L929S cells. d By contrast, staurosporine-induced apoptosis of L929S cells at 37oC exhibited condensation and increased whole cell thickness reaching ~12 μm. e A summarized graph shows the changes in area, thickness and volume of COS7 and L929S cells during BCD and apoptosis.
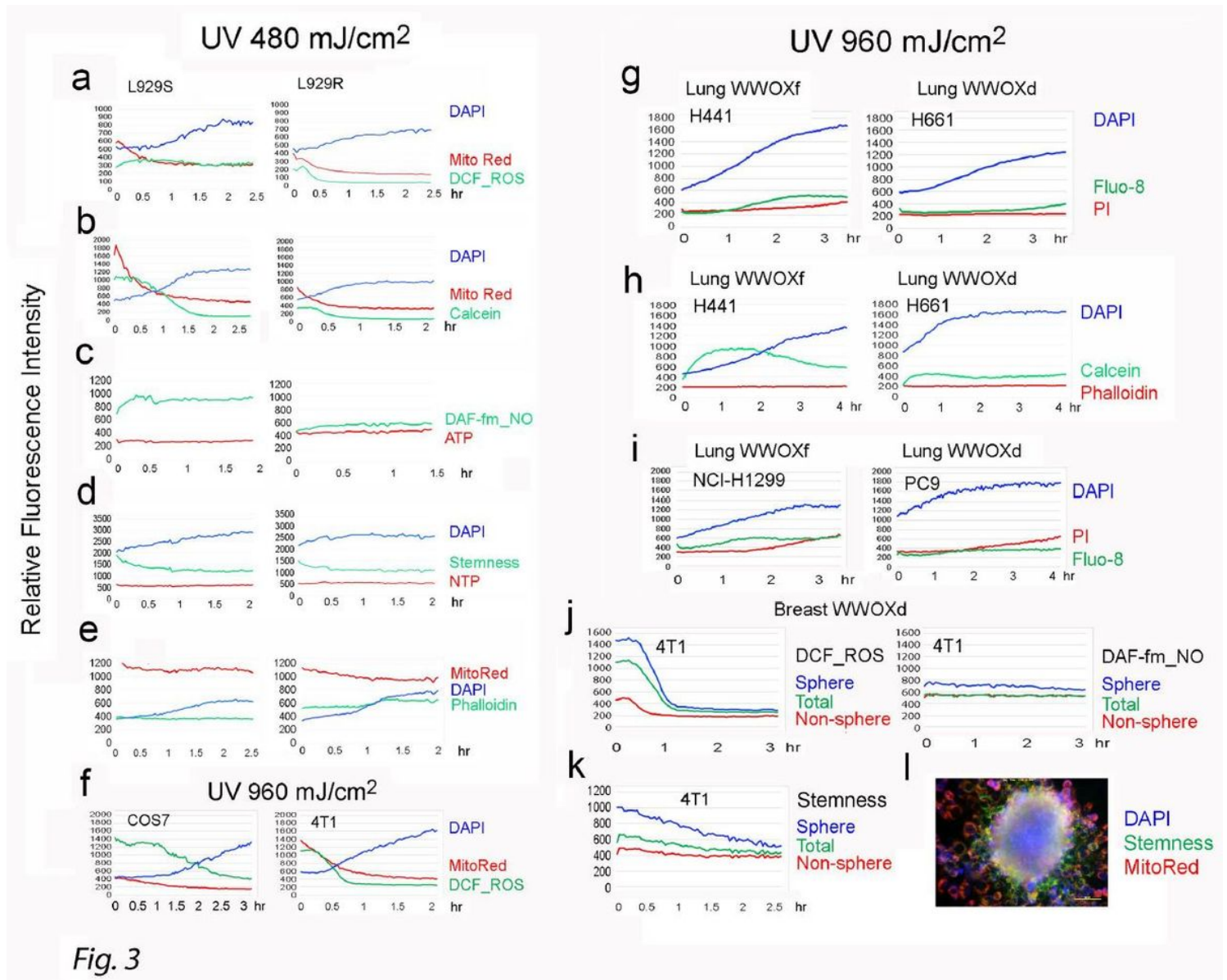

Fig. 3

Figure 3

UV induces cellular response in the coculture of WWOXf and WWOXd cells. a-e L929S and L929R cells were exposed to UV, followed by imaging with time-lapse microscopy at room temperature. Time-related changes in UV-treated cells were measured, including mitochondrial membrane potential (Mitotracker Red) (a, b, e), calcein retain in surviving cells (b), production of ROS (Dichlorofluorescein dye) (a) and NO (DAF-fm diacetate dye) (c), cell stemness (BioTracker Green Pluripotent Stem Cell dye) (d), and stress fiber formation (Phalloidin green dye) (e). Additionally, ATP (BioTracker ATP Red Live Cell dye) and NTP (BioTracker Red NTP Transporter) levels were measured (c,d). F ROS and mitochondrial membrane potential were measured in WWOXf COS7 and WWOXd 4T1 cells. g-i Calcein retention, calcium influx

(green Fluo-8 dye), stress fiber formation, and cell death (Propidium iodide) were measured in indicated lung cancer cells. j, k Breast 4T1 cells were measured at their sphere and non-sphere areas in the 4T1 cells for the ROS, NO, and stemness. l A typical 4T1 cell sphere is shown. m-q Measuring the indicated changes caused by UV in the coculture of L929S with L929R or MDA-MB-231 cells. Stress fiber formation was faster in L929R than in L929S cells (n). Nuclear stain DAPI was added to the cell culture for all experiments.

Fig. 4

Figure 4

p53, WWOX and p38 are involved in UV-mediated nuclear bubbling and calcium influx in WWOXf HCT116 cells. a In the control groups (a1, 2), exogenous medium, PBS, or normal rabbit serum (NRS; 1:250 dilution) had no effects in retarding the UV-initiated nuclear bubbling (red arrow) and calcium influx in HCT116 cells. Normal rabbit serum (NRS) sustained the increase in calcium influx with time (a3). EGTA at 200 μM did not block calcium influx, but the first bubbling time was prolonged to approximately 48 min (a4). Inhibitor of NO synthase Nω-LAME at 300 μM retarded the nuclear bubbling but had no effect on calcium influx (a5). b In the p53 group, compared to the p53 monoclonal antibody (b1), polyclonal antibodies against p53 effectively blocked nuclear bubbling and calcium influx (b2). p53β (b3) and p53β (b4) retarded the nuclear bubbling and sustained the calcium influx. c In the TβR group, when cells were

treated with a chemical inhibitor for TβRI (c1), monoclonal antibody against TβRII (c2), or an inhibitor SD208 for TβRI (c3), had no apparent inhibitory effects on nuclear bubbling and calcium influx. d In the WWOX group, WWOX7-21 or WWOX7-11 peptide had no apparent effects on nuclear bubbling and calcium influx (d1, 2). Mutant peptides WWOX7-11(A7R) and WWOX7-11(G7R) did not have inhibitory effects (d3, 4). Three antibodies against indicated different regions of WWOX retarded calcium influx but had no effect on nuclear bubbling (d5-7). Antibodies against phosphorylated WWOX protein revealed that pY33, pT12 and pS14-WWOX were most effective in blocking calcium influx and nuclear bubbling (d8-12). Isoform WWOX2 antibody suppressed calcium influx but failed to block nuclear bubbling (d13). E In the Hyal-2 group, all antisera against Hyal-2 and pY216-Hyal-2 did not effectively block nuclear bubbling and partially inhibited calcium influx (e1-4). Membrane Hyal-2 acts as a cognate receptor for both TGF-β1 and hyaluronan to signal together with WWOX and Smad4 for exerting growth enhancement or suppression13,28. f p38 inhibitor SB203580 strongly suppressed both nuclear bubbling and calcium influx.
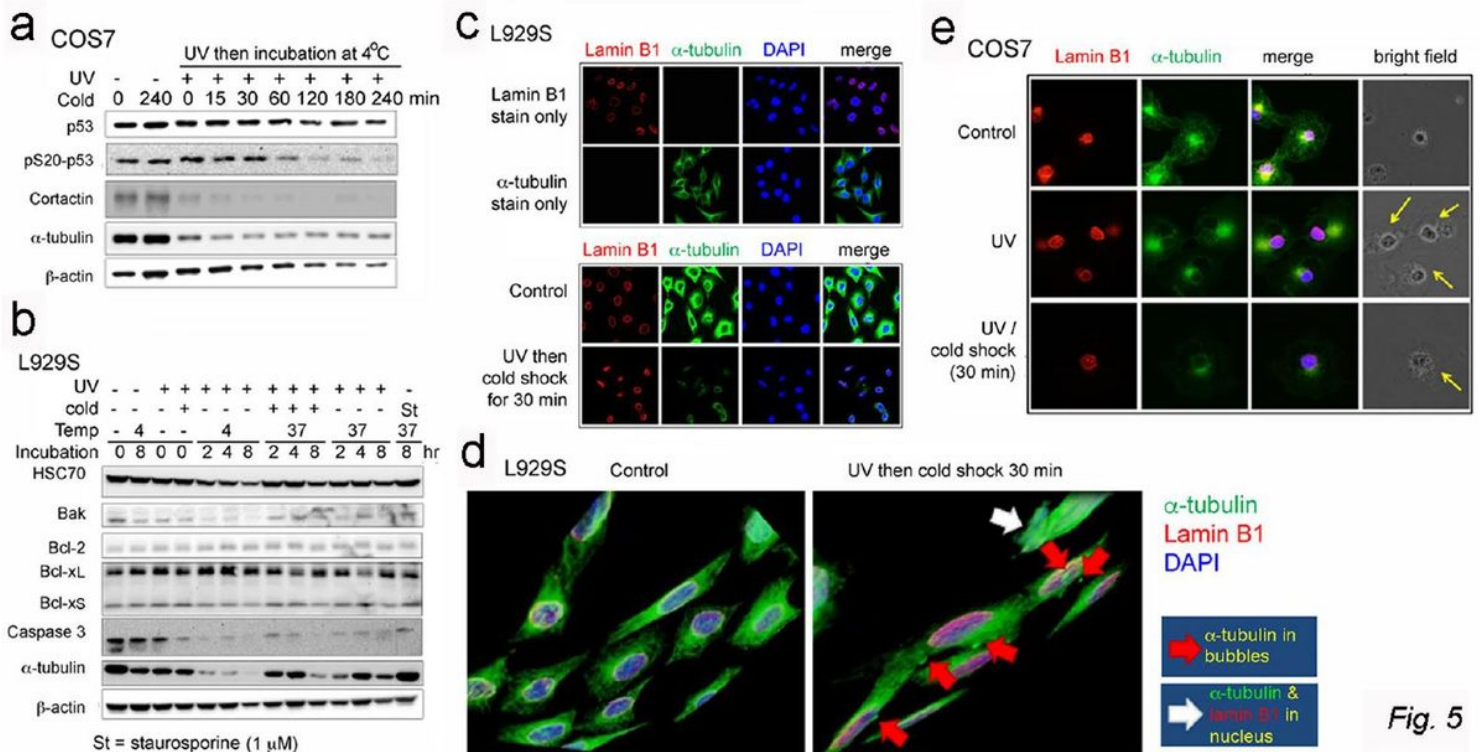

Figure 5

UV/cold shock dramatically downregulates housekeeping proteins and others, and causes leaking of α-tubulin to the enlarging bubbles. a COS7 cells were exposed to UV (480 mJ/cm2) and then cold shock for indicated times. Downregulation of cortactin, α-tubulin and actin is shown. p53 phosphorylation at S20 is reduced with time. b L929S cells were exposed to UV irradiation (480 mJ/cm2) and then cold shock (4oC) for 5 min, and were subsequently incubated at 4 or 37oC for indicated times. Whole cell lysates were prepared for SDS-PAGE and Western blotting analysis. c L929S cells were fixed with 3.7% paraformaldehyde and permeabilized with Triton-X100. Cells were stained with lamin B1 and α-tubulin for imaging by confocal microscopy (top panel). Cells were also treated with or without UV/cold shock.

Downregulation of α-tubulin is shown (bottom panel; magnification: 1000X). d The confocal image was built from Z stacks (left panel). Presence of α-tubulin in the bubbles are shown (right panel; red arrows). The bubble also contained α-tubulin and materials from the nucleus. e α-Tubulin failed to relocate to the bubbles (yellow arrows) in COS7 cells during BCD (magnification: 400X).
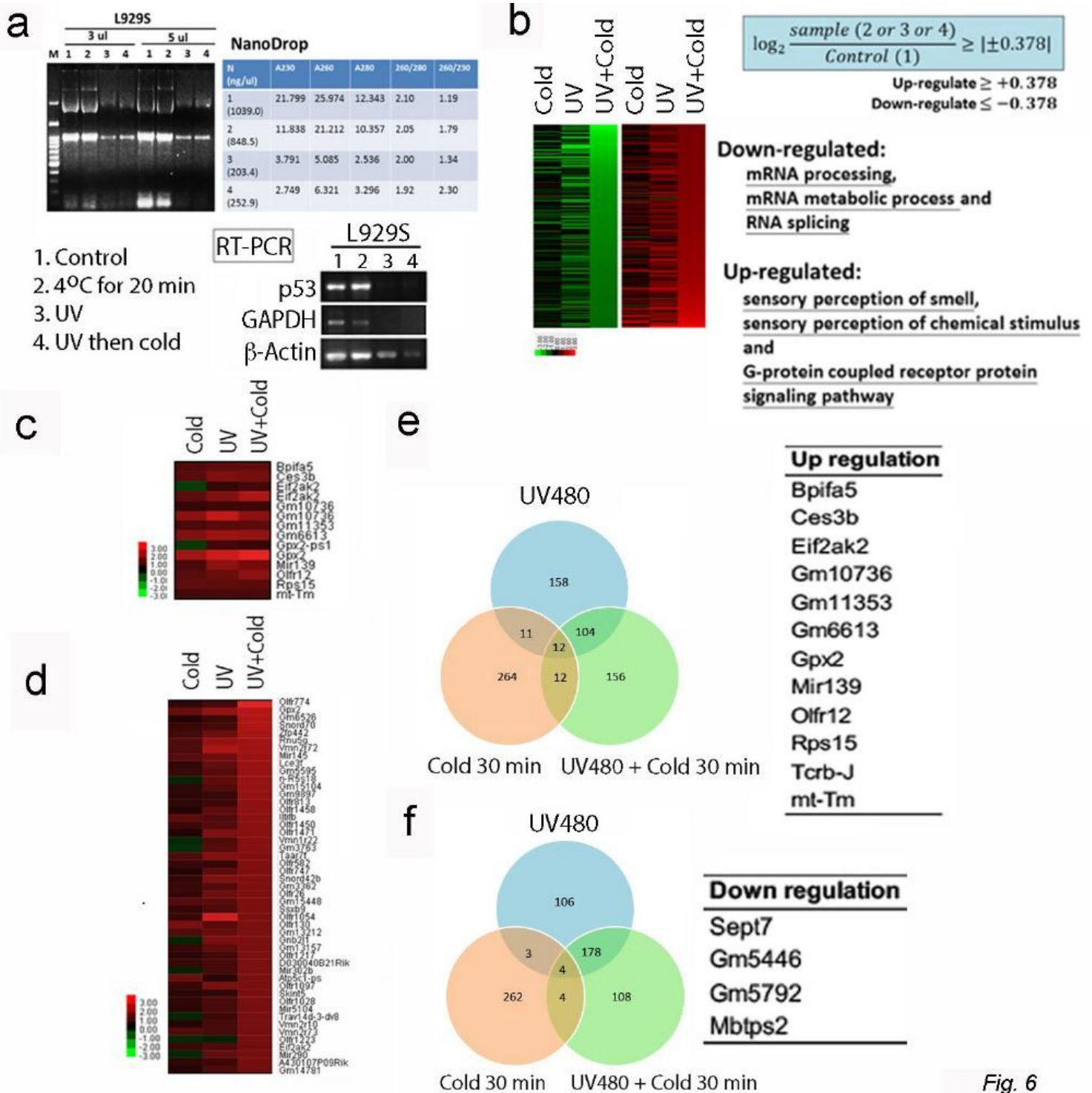

Fig. 6

Figure 6

UV/cold shock shuts down the mRNA processing machinery in L929S cells. a L929S cells were treated with UV (480 mJ/cm2) and/or cold shock (4oC for 20 min), followed by RNA purification from cells and

subjected to analysis by RNA gel electrophoresis and NanoDrop quantification. Total RNA was decreased rapidly after UV exposure. By RT-PCR, UV was shown to effectively suppress the gene expression for p53, NADPH and β-actin. b-f Gene expression profiling analysis revealed showed that mRNA processing, mRNA metabolic process and RNA splicing were down-regulated (b). However, sensory perception of smell, sensory perception of chemical stimulus and G-protein coupled receptor protein signaling pathway were up-regulated (b). Gene expression of glutathione peroxidase 2 (Gpx2) and eukaryotic translation initiation factor 2-alpha kinase 2 (Eif2ak2) were both increased after treating with UV/cold shock in L929S cells (c-f).
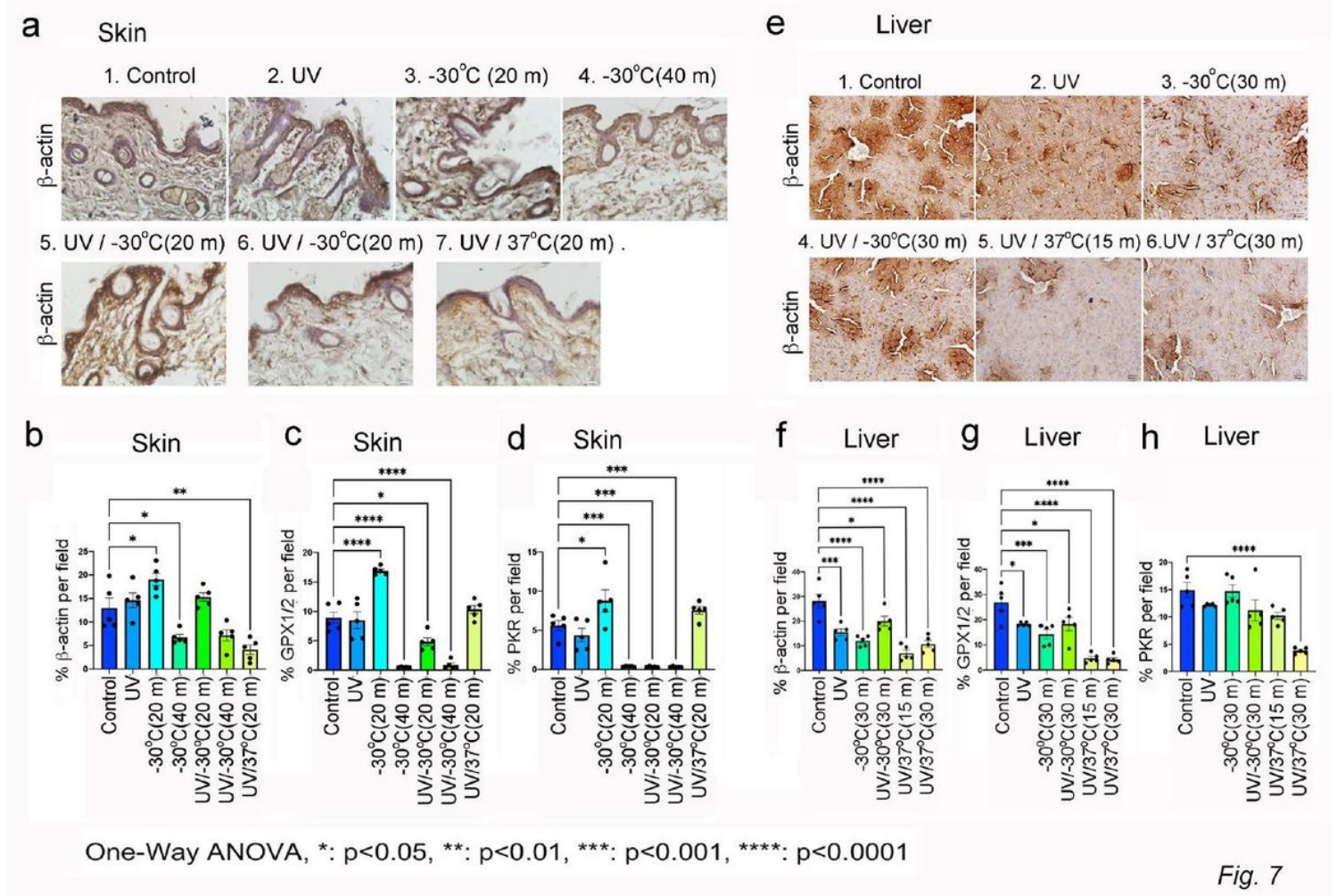

Fig. 7

Figure 7

Rapid suppression of protein expression from skin to liver in the UV/cold shock-treated hairless mice. Hairless mice were exposed to UV (960 mJoule/cm2) and then kept in a -30o C or 37o C chamber for indicated times. Mice were then sacrificed. Orangs were harvested and processed for immunohistochemistry using specific antibodies. a-d In the skin tissue sections, expression of β-actin, GPX1/2, PKR, α-tubulin, and TRAF2 is shown. See additional protein expression data in Fig. S8. e-h Under similar conditions, protein expression in the mouse liver was determined by immunohistochemistry. Also, see data in the Supplementary Fig. 9.
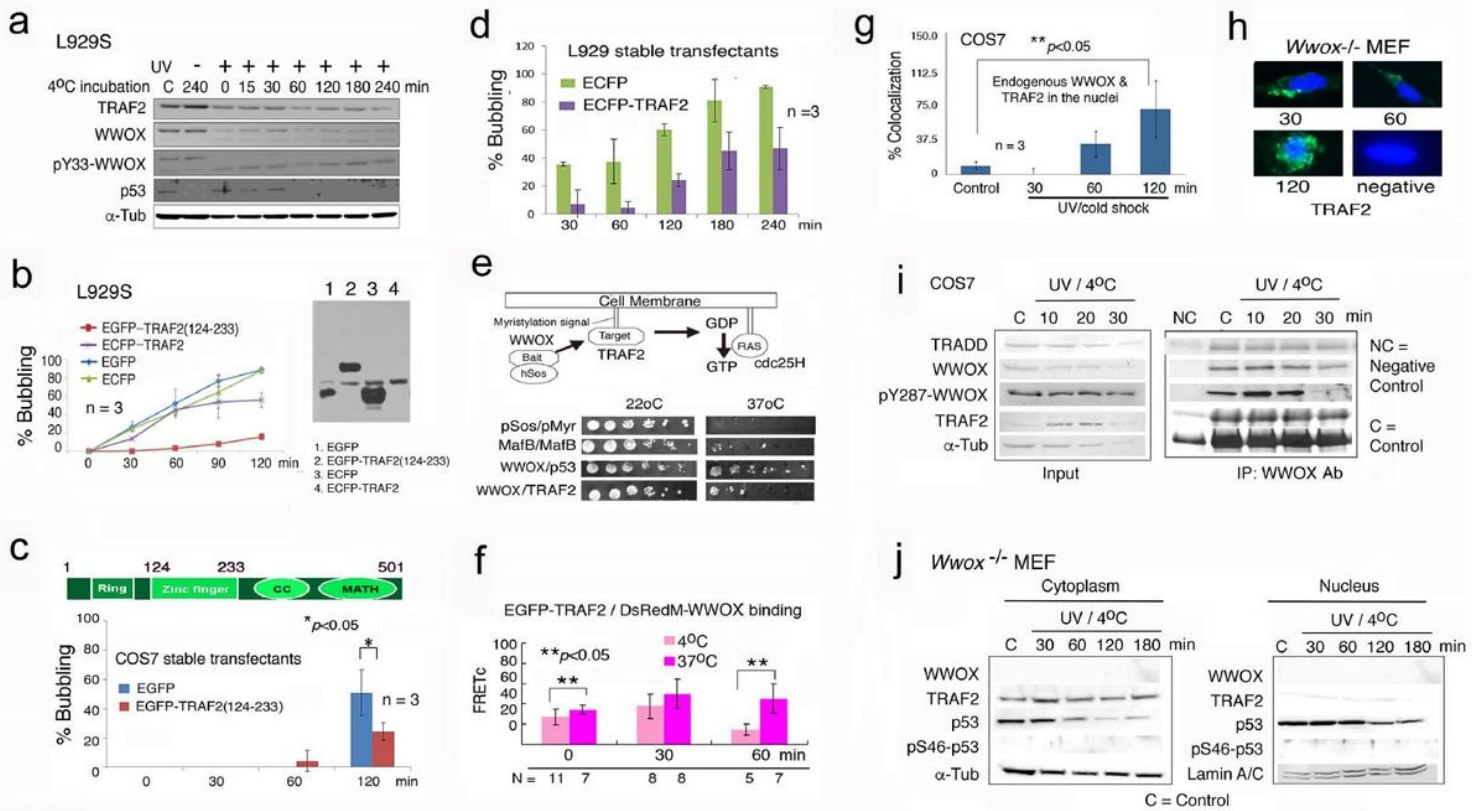
Figure 8

UV/cold shock induces TRAF2/WWOX complex to co-translocate to the nucleus. a L929S cells were exposed to UV (480 mJ/cm2) and then cold shock at 4°C for indicated times, and whole cell lysates harvested. Downregulation of WWOX, TRAF2 and α-Tubulin was about 50%. b L929S cell stable transfectants were established. EGFP-TRAF2(124-233) strongly suppressed UV/cold shock-induced BCD. The full-length ECFP-TRAF2 was not expressed and did not exhibit an inhibitory activity. c, d Inhibitory activity is shown with EGFP-TRAF2(124-233) and ECFP-TRAF2 to block BCD in stable transfectants of COS7 and L929S cells, respectively. e By Cytotrap yeast two-hybrid analysis, binding of WWOX with TRAF2 is shown. In positive controls, the complex formation of p53/WWOX and MafB/MafB is demonstrated. f By FRET microscopy, binding of EGFP-TRAF2 with DsRedM-WWOX was stably increased in UV/cold shock-treated COS7 cells at 37oC, whereas the binding was reduced at 4oC in 60 min. DsRedM = monomeric DsRed. g UV/cold shock induces nuclear co-localization of endogenous WWOX and TRAF2 in COS7 cells. h Endogenous TRAF2 in Wwox-/- knockout MEF cells did not undergo nuclear relocation in response to UV/cold shock. A representative data is shown from more than 200 cells. i UV/cold shock induced the dissociation of the WWOX/TRAF2 complex in 30 min in COS7 cells, as determined by co-immunoprecipitation. j In the absence of WWOX, UV/cold shock did not induce translocation of cytosolic TRAF2 to the nucleus in Wwox-/- MEF cells, whereas p53 nuclear translocation occurred.

Supplementary Files

This is a list of supplementary files associated with this preprint. Click to download.

- SupplementaryTable1.pdf
- VideoS1MCF7UV48dapipifluo820xrt2minframend11165.mp4
- VideoS5.L929sUVcoldshock216hrsubmission.mp4
- VideoS6L929sstaurosporine2uM37oC10hr.mp4
- VideoS7.L929s4800UVcoldshockfor5minincubatedAt37C2.24hr.mp4
- VideoS12cfpcfpforgreenfluo8channelUV9620xrt2minframend703fluo8.mp4
- VideoS913.L929sControl37C2.8hr.mp4
- VideoS812.L929sControl37C.8hr.mp4
- VideoS4.COS7UVcold216hr.submission.mp4
- VideoS104T1oxflcfpforgreenfluo8channelUV9620xrt2minframend700.mp4
- VideoS3.COS7UVcold116hr.mp4.mp4
- VideoS2MDAMB231UV480dapipifluo820xrt2minframend11171.mp4
- VideoS11.4T1oxflcfpforbluechannelUV9620xrt2minframend700.mp4
- VideoS13cfpforbluechannelUV9620xrt2minframend703.mp4
- SupplementaryInformation.pdf